OPTICA

Cryogenic integrated spontaneous parametric down-conversion

Nina Amelie Lange,[1,*] Jan Philipp Höpker,[1] Raimund Ricken,[2] Viktor Quiring,[2] Christof Eigner,[2] Christine Silberhorn,[2] and Tim J. Bartley[1]

[1]Mesoscopic Quantum Optics, Department of Physics, Paderborn University, Warburger Str. 100, 33098 Paderborn, Germany
[2]Integrated Quantum Optics, Department of Physics, Paderborn University, Warburger Str. 100, 33098 Paderborn, Germany
*Corresponding author: nina.amelie.lange@upb.de

Received 12 October 2021; revised 6 December 2021; accepted 8 December 2021; published 14 January 2022

Scalable quantum photonics relies on interfacing many optical components under mutually compatible operating conditions. To that end, we demonstrate that spontaneous parametric down-conversion (SPDC) in nonlinear waveguides, a standard technology for generating entangled photon pairs, squeezed states, and heralded single photons, is fully compatible with cryogenic operating conditions required for superconducting detectors. This is necessary for the proliferation of integrated quantum photonics in integration platforms exploiting quasi-phase-matched second-order nonlinear interactions. We investigate how cryogenic operation at 4 K affects the SPDC process by comparing the heralding efficiency, second-order correlation function, and spectral properties with operation at room temperature.

https://doi.org/10.1364/OPTICA.445576

Generation, manipulation, and detection of quantum light are based on a wide range of photonic quantum technologies [1–3]. In a fully integrated platform, each technology must be mutually compatible [2], not only with regard to the optical degrees of freedom of interest, but also their operating conditions. While nonlinear optics, in particular, frequency conversion and electro-optic manipulation, is optimized for operation under ambient conditions, many quantum photonic technologies, in particular, superconducting single-photon detectors and low-noise single emitters, require cryogenics [4]. To enable mutual integration of these components, it is necessary to adapt existing techniques and technologies to be functional in the same environment.

One important and well-established technique for generating nonclassical light under ambient conditions is spontaneous parametric down-conversion (SPDC) [5–7]. In various configurations, this can be used to generate heralded single photons [8], entangled states [9], squeezed states [10], and, in combination with single-photon detection as a non-Gaussian operation, non-Gaussian states such as Schrödinger cat states [11]. SPDC has been used extensively in materials such as lithium niobate, in which phase-matching is achieved through periodic inversion of the spontaneous polarization of the crystal [12–15]. Furthermore, waveguides can be fabricated in this material, further enhancing the nonlinear interaction and allowing additional control of the phase-matching properties. Titanium in-diffused waveguides in particular have shown a wide range of functionality combining quantum light sources and electro-optic processing on low-loss chips [16–19]. Demonstrating this functionality under cryogenic operating conditions is therefore vital to augment the range of integrated circuits that can be implemented.

In this Letter, we show that cryogenic SPDC is indeed possible, and discuss variations to the phase-matching caused by the large temperature change. We show photon pair emission and joint spectral measurements when the sample is cooled to 4.7 K. This is directly compared to the same sample at room temperature. The SPDC process we consider is quasi-phase-matched type-II SPDC in titanium in-diffused waveguides in periodically poled lithium niobate [18,20]. This interaction results in photons generated in orthogonal polarization modes, traditionally called signal and idler. In this configuration, the signal and idler modes can be deterministically separated, and the measurement of one photon can be used to herald the presence of the other.

To understand SPDC under cryogenic conditions, we study the temperature-dependent variations in the spectral properties of the signal and idler, which are dictated by energy and momentum conservation. Energy conservation is specified by the pump beam; it is independent of the sample temperature T. In contrast, momentum conservation is determined by the crystal length, its dispersion, and the poling period, all of which exhibit temperature dependence.

Momentum conservation is governed by the difference in propagation constants k of the interacting modes, given by

$$\Delta k = k_p(\lambda_p) - k_s(\lambda_s) - k_i(\lambda_i), \tag{1}$$

where λ is the wavelength, and subscripts p, s, i denote the pump, signal, and idler modes, respectively. In general, due to the dispersion properties of the material, the interacting modes are not phase-matched, i.e., $\Delta k \neq 0$. However, in many second-order materials, momentum conservation can be achieved by introducing an additional contribution to the momentum, arising from a periodic inversion of the crystal symmetry, known as periodic poling [13]. Equation (1) is thus modified to $\Delta k' = \Delta k \pm 2\pi/\Lambda$, where Λ is the poling period of the crystal. Thus, Λ can be chosen such that $\Delta k' = 0$ for a given combination of signal and idler wavelengths $\lambda_{s,i}$.

By writing $k = 2\pi n/\lambda$, where n is the refractive index, we can account for the temperature dependence of the interaction, as well as the thermal contraction of the poling period $\Lambda(T)$. Without loss of generality, the phase-matching condition may be written as

$$\frac{n_{\mathrm{TE}}(\lambda_p, T)}{\lambda_p} - \frac{n_{\mathrm{TE}}(\lambda_s, T)}{\lambda_s} - \frac{n_{\mathrm{TM}}(\lambda_i, T)}{\lambda_i} - \frac{1}{\Lambda(T)} = 0, \quad (2)$$

where $n_{\mathrm{TE}}(\lambda, T)$ and $n_{\mathrm{TM}}(\lambda, T)$ are the temperature-dependent effective refractive indices of the transverse-electric (TE) and transverse-magnetic (TM) polarized modes, respectively.

For the following calculations, we use temperature-dependent effective refractive index data based on Sellmeier equations for bulk lithium niobate [21,22], which are extrapolated for low temperatures and modified for the waveguide geometry. An additional correction is applied to the extrapolated data, which is empirically obtained by measuring the second-harmonic generation (SHG) spectra during the cool-down of the waveguide (for details on the extrapolation and measurement procedure, see [23]). Empirical data for the thermal expansion coefficient of lithium niobate in the y direction is available for $T \geq 60$ K [24]. The expansion coefficient tends to zero at 0 K; therefore, when extrapolating for temperatures below 60 K, the sample length and the poling period can be assumed constant.

We calculate the changes in the phase-matching properties for temperatures in a range from 300 K down to 0 K by computing the signal and idler wavelength pair (λ_s, λ_i), which fulfills energy conservation and temperature-dependent momentum conservation (Eq. 2). The calculation is performed for a pump wavelength of $\lambda_p = 778$ nm and for four poling periods, which are chosen to enable spectrally degenerate SPDC around room temperature (see Fig. 1). From room temperature to 4 K, the wavelengths of the signal and idler are expected to shift by about 90 nm, due to the dispersion of the waveguide.

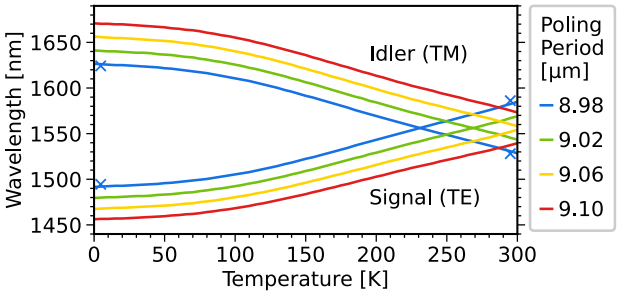

Fig. 1. Theoretical temperature dependence of signal and idler wavelengths for a pump wavelength of $\lambda_p = 778$ nm, displayed for different poling periods. The crosses show our spectral measurement results for a poling period of 8.98 μm.

In fact, the temperature dependence of phase-matching is often exploited to achieve a desired nonlinear interaction, by placing the sample on a temperature controlled mount [18]. Under cryogenic operation, thermal tuning is not possible, and therefore Fig. 1 shows the importance of achieving the correct poling period for operation at a fixed temperature.

These calculations account for macroscopic, well-defined changes to the refractive indices. In many second-order materials, other temperature-dependent effects may change the resulting spectral behavior. In the case of lithium niobate, the material is pyroelectric, piezoelectric, and photorefractive [25], meaning temperature changes (rather than absolute temperature) and optical power can locally alter the refractive index and therefore the phase-matching. Previous work has shown this may be a transient effect during temperature cycling, which nevertheless exhibits stable operation under a constant temperature [23].

Building on these calculations, we experimentally investigated the phase-matching and other source properties of a lithium niobate waveguide chip operated under cryogenic conditions. The waveguide sample is fabricated by titanium in-diffusion into a z-cut congruently grown uncoated lithium niobate chip. These waveguides support low-loss propagation of TE and TM polarization modes, with losses down to 0.03 dB/cm at 1550 nm under room temperature operation [16]. A single chip of length 24.4 mm contains 16 groups of three straight waveguides, and each waveguide group is periodically poled with poling periods from 8.98 to 9.12 μm in increments of 0.02 μm. At room temperature, these poling periods allow for degenerate type-II SPDC with the signal and idler wavelengths in the telecom C-band.

The experimental setup is shown in Fig. 2. We place our waveguide sample inside a free-space coupled cryostat, with a base temperature of 4.7 K. The waveguide end facets are optically accessible through transparent windows, which allows us to couple the laser beam to the waveguide with aspheric lenses positioned outside the cryostat. The in- and out-coupling lenses are anti-reflection coated for the pump and downconverted light, respectively. We can move the sample inside the cryostat with a motorized mount to change between waveguides and therefore different poling periods at any time.

To prepare the pump beam for the SPDC process, we use the SHG signal from a bulk periodically poled MgO-doped lithium niobate (MgO:PPLN) crystal (heated to about 70°C). We pump the SHG with an ultrashort pulsed infrared laser with a repetition rate of 80 MHz. The pump spectrum exhibits a Gaussian shape with a central wavelength of (778.0 ± 0.1) nm and a bandwidth of (3.2 ± 0.1) nm. We use a pump power of about 200 μW, resulting in an average photon-pair generation probability well below 0.1.

We set the polarization of the pump light to excite the TE waveguide mode to pump type-II SPDC. Following the chip,

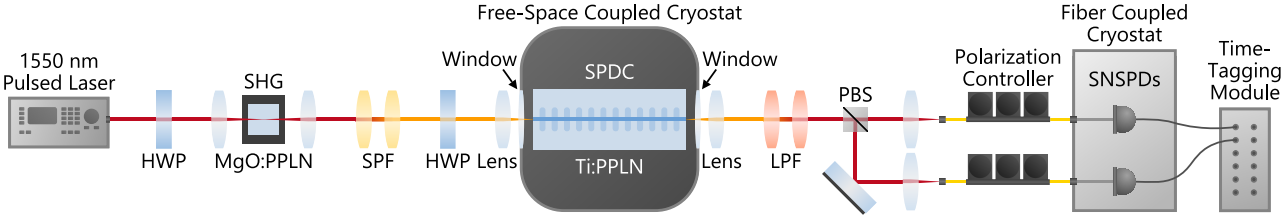

Fig. 2. Experimental setup to measure SPDC photons, generated in the periodically poled lithium niobate waveguide, which is positioned inside a free-space coupled cryostat. HWP, half-wave plate; MgO:PPLN/Ti:PPLN, MgO-doped/titanium-indiffused periodically poled lithium niobate; SPF/LPF, short-pass/long-pass filter; PBS, polarizing beam splitter.

long-pass filters (LPFs) remove the high-energy pump beam, and the signal and idler photons are separated via a broadband polarizing beam splitter (PBS) before being coupled into single-mode fibers. We use superconducting nanowire single-photon detectors (SNSPDs) located in a separate cryostat to measure the photons. Single counts and coincidences of the signal and idler are recorded with a time-tagging module.

We characterize our SPDC source at room temperature (295 K) and under cryogenic conditions (4.7 K). The free-space coupled cryostat shown in Fig. 2 allows us to use exactly the same setup for both measurements. Moreover, it enables us to optimize the beam coupling to the waveguide end facets at any time. We characterize our source with regard to the spectral properties and the source performance metrics.

We investigate the spectral properties by employing a home-built scanning-grating spectrometer setup (for details, see Supplement 1). We measure the marginal spectra by inserting one spectrometer into the signal or idler path in front of the polarization controller. Afterwards, we perform a measurement of the joint spectral intensity (JSI) by applying one spectrometer to the signal path, and another one to the idler path. These results are shown in Fig. 3.

Our results show that cryogenic operation of SPDC is possible and that the spectral properties behave as expected. For both measurements, the marginal spectra exhibit a Gaussian shape, and the JSI is represented by an elongated ellipse, corresponding to spectral correlations of the signal and idler. The obtained central wavelengths of the signal and idler are summarized in Table 1. The measured wavelengths are in very good agreement with our simulation of a wavelength shift of about 90 nm (compare Fig. 1).

To simulate the JSI, we take into account the pump wavelength and spectral width, the poling period, and the effective refractive indices. We keep the effective length of the waveguide as a variable parameter and perform an optimization until the simulation fits the measured JSI best (for details, see Supplement 1). The effective length accounts for position dependence of the refractive indices in Eq. (2) due to local perturbations, which means that the phase-matching condition is not necessarily satisfied at all positions along the waveguide. These localized perturbations arise from the interplay among the photorefractive, pyroelectric, and piezoelectric effects during temperature cycling [23]. According to the optimization, the effective length decreases from (7.3 ± 0.3) mm to (3.65 ± 0.05) mm when cooling down the sample. Our simulations show that the decreased effective length corresponds to a broadening of the phase-matching function, and therefore the JSI (see Fig. S2 in Supplement 1). This broadening is clearly visible in our measured JSI shown in Fig. 3.

Furthermore, our simulations verify the change in the angle of the JSI. This change is caused by the overlap of the unchanged pump distribution function with the temperature-dependent phase-matching function. The latter is determined by the temperature-dependent dispersion of the waveguide and the reduction in effective length. The change is also visible in the bandwidths of the marginal spectra: the signal bandwidth decreases during cool-down from $\Delta\lambda_s = (32.08 \pm 0.28)$ nm to $\Delta\lambda_s = (27.4 \pm 0.5)$ nm, while the cryogenic idler bandwidth $\Delta\lambda_i = (17.94 \pm 0.21)$ nm is almost unchanged compared to $\Delta\lambda_i = (17.27 \pm 0.10)$ nm at room temperature.

In addition to the spectral features of the cryogenic source, we compare the source performance metrics at both room temperature and 4.7 K. We study the brightness B, Klyshko (heralding) efficiency η_{Klyshko}, coincidences-to-accidentals ratio (CAR), and heralded autocorrelation function $g_h^{(2)}(0)$. These results are summarized in Table 1.

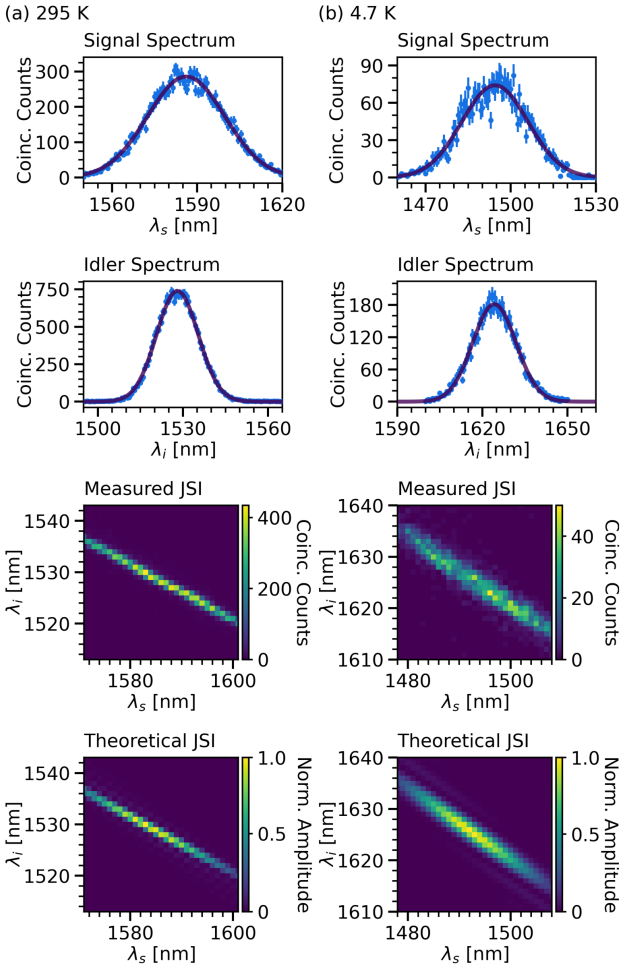

Fig. 3. Experimental results for the spectral measurements of the signal and idler photons, together with the simulated joint spectral intensity (JSI) for a room temperature poling period of 8.98 μm (for higher resolution, see Supplement 1). The marginal spectra and the JSI are measured (a) at room temperature and (b) under cryogenic conditions. The solid line in each marginal spectrum represents a Gaussian fit to the measurement data, and the errorbars correspond to Poisson errors.

The brightness of our source is given by $B = C_{si}/P_{\text{trans}}$, where C_{si} is the coincidence rate of the signal and idler, and P_{trans} is the transmitted pump power. The brightness of a waveguide source scales with the effective length of the sample [26]. Our spectral measurements indicate a reduction in effective length by approximately half, which indeed results in a commensurate reduction in brightness by the same factor.

The reduced brightness also affects the signal-to-noise ratio of the source, which is evident in the Klyshko efficiency $\eta_{\text{Klyshko}} = \sqrt{C_{si}^2/(C_s C_i)}$, where C_s and C_i are the single count rates. Our results show that Klyshko efficiency at cryogenic temperatures is decreased by a factor of roughly 1.8 compared to room temperature, consistent with the reduced brightness at constant noise (for details, see Supplement 1).

A decrease in the signal-to-noise ratio is further verified by investigating the CAR, which, in the low generation probability regime, is given by $\text{CAR} = (C_{si} R_{\text{rep}})/(C_s C_i)$, where R_{rep} is the

Table 1. Comparison of Our Source Performance at Room Temperature (295 K) and under Cryogenic Conditions (4.7 K)[a]

	λ_s [nm]	λ_i [nm]	L_{eff} [mm]	Brightness $B[\frac{\text{pairs}}{\text{smW}}]$	η_{Klyshko}[%]	CAR	$g_h^{(2)}(0)$
295 K	1586.14 ± 0.12	1528.05 ± 0.04	7.3 ± 0.3	$(6.6 \pm 0.3) \times 10^5$	8.47 ± 0.03	53.9 ± 0.2	0.033 ± 0.004
4.7 K	1494.45 ± 0.19	1624.24 ± 0.09	3.65 ± 0.05	$(3.3 \pm 0.1) \times 10^5$	4.77 ± 0.03	32.9 ± 0.2	0.07 ± 0.01

[a]The table shows the phase-matched signal and idler wavelengths (λ_s, λ_i), effective crystal length L_{eff}, brightness B, Klyshko efficiency η_{Klyshko}, coincidences-to-accidentals ratio CAR, and heralded autocorrelation function $g_h^{(2)}(0)$.

laser repetition rate. Compared to room temperature, we observe a lower CAR value at 4.7 K by a factor of approximately 1.6, which is consistent with the reduced effective length.

Finally, we measured the heralded autocorrelation function to investigate the photon number purity of our source. We added a 50:50 fiber beam splitter to the signal path in front of the polarization controller. For this configuration, the heralded autocorrelation function is calculated by $g_h^{(2)}(0) = (C_{s_1 s_2 i} C_i)/(C_{s_1 i} C_{s_2 i})$, where $C_{s_1 i}$ and $C_{s_2 i}$ are the coincidence rates of the two signal photons with the idler photons, and $C_{s_1 s_2 i}$ are the threefold coincidences. The heralded $g_h^{(2)}(0)$ remains well below the classical threshold of one, but increases by a factor of two with respect to the room temperature value.

At cryogenic temperatures, all figures of merit are consistent with a reduction in the signal-to-noise ratio by a factor of two, compared with room temperature operation. We expect this decrease to be due to photorefractive effects, which distort the guided mode [27], depending on laser intensity and exposure time. This distortion reduces conversion efficiency. Nevertheless, the figures of merit demonstrate a high-quality SPDC source at cryogenic temperature.

Demonstrating mutual compatibility of operating conditions is crucial for the proliferation of quantum technologies. As part of this process, we demonstrated that SPDC in quasi-phase-matched waveguides is compatible with the operating temperatures required for superconducting detectors. Despite changing the operating temperature by nearly two orders of magnitude, the source remained fully operational: our results indicate that cryogenics principally affect the (spectral) modes that the SPDC populates, rather than the quantum states themselves. Building on this, a thorough characterization of the linear losses and spatial mode profiles will be beneficial to understand the impact of cryogenics on the guided modes and the quantum states that occupy them.

Funding. Bundesministerium für Bildung und Forschung (13N14911).

Disclosures. The authors declare no conflicts of interest.

Data Availability. Data underlying the results presented in this Letter are not publicly available at this time but may be obtained from the authors upon reasonable request.

Supplemental document. See Supplement 1 for supporting content.

REFERENCES

1. J. L. O'brien, A. Furusawa, and J. Vučković, Nat. Photonics **3**, 687 (2009).
2. J. Wang, F. Sciarrino, A. Laing, and M. G. Thompson, Nat. Photonics **14**, 273 (2020).
3. G. Moody, V. J. Sorger, P. W. Juodawlkis, *et al.*, J. Phys. Photon. (to be published).
4. M. D. Eisaman, J. Fan, A. Migdall, and S. V. Polyakov, Rev. Sci. Instrum. **82**, 071101 (2011).
5. J. Rarity, P. Tapster, and E. Jakeman, Opt. Commun. **62**, 201 (1987).
6. Y. Shih and C. O. Alley, Phys. Rev. Lett. **61**, 2921 (1988).
7. Z. Ou and L. Mandel, Phys. Rev. Lett. **61**, 50 (1988).
8. C. Hong and L. Mandel, Phys. Rev. Lett. **56**, 58 (1986).
9. P. G. Kwiat, K. Mattle, H. Weinfurter, A. Zeilinger, A. V. Sergienko, and Y. Shih, Phys. Rev. Lett. **75**, 4337 (1995).
10. L.-A. Wu, H. Kimble, J. Hall, and H. Wu, Phys. Rev. Lett. **57**, 2520 (1986).
11. A. Ourjoumtsev, R. Tualle-Brouri, J. Laurat, and P. Grangier, Science **312**, 83 (2006).
12. S. Tanzilli, H. De Riedmatten, H. Tittel, H. Zbinden, P. Baldi, M. De Micheli, D. B. Ostrowsky, and N. Gisin, Electron. Lett. **37**, 26 (2001).
13. S. Tanzilli, W. Tittel, H. De Riedmatten, H. Zbinden, P. Baldi, M. DeMicheli, D. B. Ostrowsky, and N. Gisin, Eur. Phys. J. D **18**, 155 (2002).
14. G. Fujii, N. Namekata, M. Motoya, S. Kurimura, and S. Inoue, Opt. Express **15**, 12769 (2007).
15. S. Krapick, B. Brecht, H. Herrmann, V. Quiring, and C. Silberhorn, Opt. Express **24**, 2836 (2016).
16. W. Sohler, H. Hu, R. Ricken, V. Quiring, C. Vannahme, H. Herrmann, D. Büchter, S. Reza, W. Grundkötter, S. Orlov, H. Suche, R. Nouroozi, and Y. Min, Opt. Photon. News **19**(1), 24 (2008).
17. P. R. Sharapova, K. H. Luo, H. Herrmann, M. Reichelt, T. Meier, and C. Silberhorn, New J. Phys. **19**, 123009 (2017).
18. N. Montaut, L. Sansoni, E. Meyer-Scott, R. Ricken, V. Quiring, H. Herrmann, and C. Silberhorn, Phys. Rev. Appl. **8**, 24021 (2017).
19. K.-H. Luo, S. Brauner, C. Eigner, P. R. Sharapova, R. Ricken, T. Meier, H. Herrmann, and C. Silberhorn, Sci. Adv. **5**, eaat1451 (2019).
20. A. Martin, A. Issautier, H. Herrmann, W. Sohler, D. B. Ostrowsky, O. Alibart, and S. Tanzilli, New J. Phys. **12**, 103005 (2010).
21. G. J. Edwards and M. Lawrence, Opt. Quantum Electron. **16**, 373 (1984).
22. D. H. Jundt, Opt. Lett. **22**, 1553 (1997).
23. M. Bartnick, M. Santandrea, J. P. Höpker, F. Thiele, R. Ricken, V. Quiring, C. Eigner, H. Herrmann, C. Silberhorn, and T. J. Bartley, Phys. Rev. Appl. **15**, 024028 (2021).
24. K. Wong, *Properties of Lithium Niobate* (INSPEC, 2002).
25. R. S. Weis and T. K. Gaylord, Appl. Phys. A **37**, 191 (1985).
26. E. Meyer-Scott, N. Prasannan, C. Eigner, V. Quiring, J. M. Donohue, S. Barkhofen, and C. Silberhorn, Opt. Express **26**, 32475 (2018).
27. J. Rams, A. A. de Velasco, M. Carrascosa, J. Cabrera, and F. Agulló-López, Opt. Commun. **178**, 211 (2000).